Electronics communication and photoinduced intramolecular electron transfer in hybrid Ru(II)-Re(I) complexes using eigenstate-based and diabatic-state-based models

Rangsiman Ketkaew*

Computational Chemistry Research Unit, Department of Chemistry, Faculty of Science and Technology, Thammasat University, Pathum Thani, 12120 Thailand

E-mail: rangsiman1993@gmail.com

Abstract

Photoinduced intramolecular electron transfer (PIET) plays a vital role in the efficiency of electronics communication in transition metal complexes for catalyzing oxidation-reduction reactions. In this work, we theoretically calculate the rate of electron transfer (ET) in $Ru^{II}-BL-Re^{I}$ hybrid complexes; where BL is bridging ligand of conjugated diene system. A brief concept of ET on the basis of the Marcus theory, which is extended to address a variety of different types of ET, is provided. We show that in the case of $Ru^{II}-BL-Re^{I}$ complex, ET involves a non-adiabatic state which thanks to a fast electronics communication between donor and acceptor connected by BL and becomes rigid complex. Single-electron transferring in $Ru^{II}-BL-Re^{I}$ complex governed by PIET constructed by potential energy curve as the change of structural transformation over time-evolution. We also investigate the mechanism of PIET involving a redox reaction in an excited state, wherein the oxidation state of Ru^{II} (donor) and Re^{I} (acceptor) changes. To access the non-adiabatic state of $Ru^{II}-BL-Re^{I}$, we use constrained density functional theory to allow ground state calculation to be performed along with geometry constraints. Our systematic study of the role of the distance of donor-acceptor separation in the kinetics of PIET elucidates an important factor paving a way for novel low-cost and efficient chemical catalysts.

1   Introduction

Highly efficient photocatalysts are required for carbon dioxide (CO_2) reduction, for example, converting CO_2 to carbon monoxide (CO).[1,2] The mixed-valence binuclear (or hybrid) complex has been widely used to speed up CO_2 reduction.[3–5] The previous study reported that an electrochemical ruthenium (Ru) catalyst to yield the CO as well as rhenium (Re) complex also has been extensively used.[4] Suntharalingam et al. studied the homogeneous metal complex and investigated mono- and bimetallic terpyridine complexes in DNA binding.[6] They found that using two transition metals is better than one metal because of its strong corresponding to the photoexcitation properties. Combining two different metal complexes, such as ruthenium (Ru) and rhenium (Re), has been achieved in order to synthesize a synergistic photocatalyst.[7] Bridging ligand (BL) has been used to link Ru and Re complexes together. Sato et al. synthesized the highly efficient $\mathbf{Ru^{II}} - \mathbf{BL} - \mathbf{Re^{I}}$ binuclear complex for CO_2 reduction and compared the photocatalytic activity of different ligand in Ru^{II} complex.[8] They found that using only the Re^{I} catalyst cannot drive this reaction because Re^{I} cannot absorb the irradiated light. The following study by Nakada et al. showed that the efficiency of $\mathbf{Ru^{II}} - \mathbf{BL} - \mathbf{Re^{I}}$ complex (in aqueous) depends on the rate of intramolecular electron transfer.[9]

The rate of electron transfer between sites in a mixed-valence complex is an important process. It has been well known that this process can be described by the Marcus theory. The covalent transition metals bridge complex is one of the good samples for studying electron transfer (ET). Nakada et al. synthesized the highly efficient $\mathbf{Ru^{II}} - \mathbf{Re^{I}}$ photocatalyst for CO_2 reduction by using C_2H_2 as a bridging ligand.[9] $[Ru^{II}(dmb)_2\text{-}(C_2H_2)\text{-}Re^{I}(CO)_3Cl]^{2+}$ complex has been synthesized and experimentally determined the rate of ET. Following this work, we studied the photoinduced intramolecular electron transfer (PIET) process of the highly efficient photosensitizer catalyst for CO_2 reduction by using density functional theory (DFT). We computed the components of Marcus equation: nuclear reorganization energy,

electron transfer matrix element or electronics coupling energy, and the Gibbs activation energy, to investigate the kinetics of PIET in the series of $[\text{Ru}^{\text{II}}(\text{dmb})_2\text{-(BL)-Re}^{I}(CO)_3\text{Cl}]^{2+}$ complexes. These three parameters were computed, and electronics properties were investigated with the dependence of BL distance.
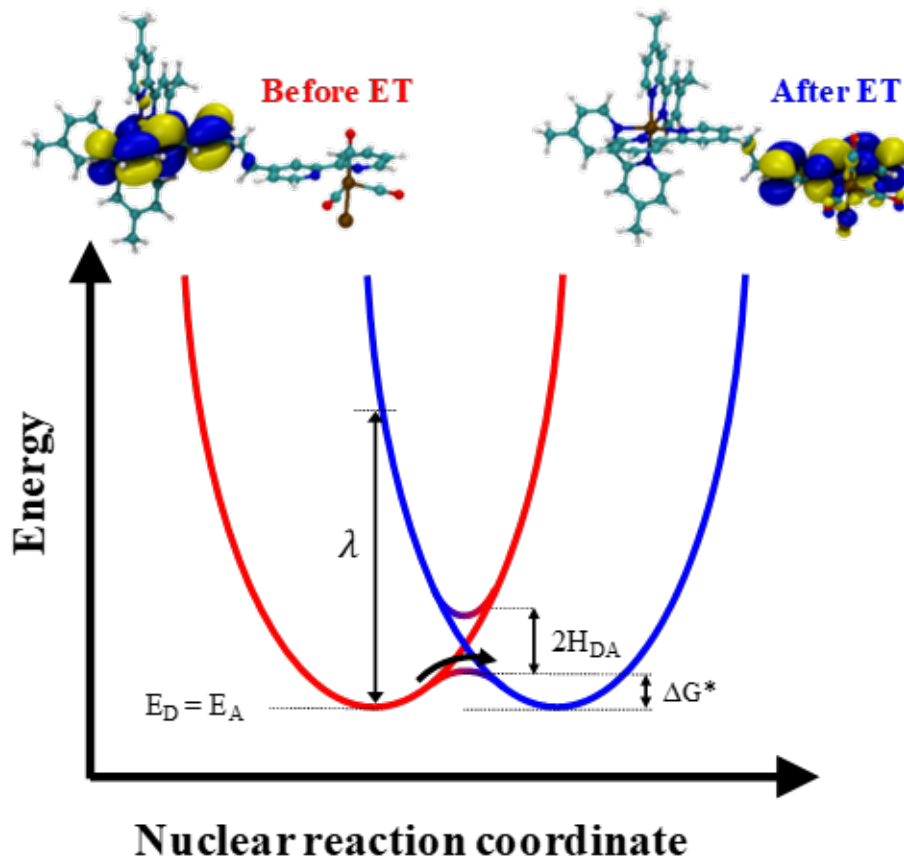

Figure 1: Potential energy curve for Marcus adiabatic and non-adiabatic states. λ is reorganization energy, H_{DA} is electron transfer matrix element, and ΔG^* is the Gibbs activation energy.
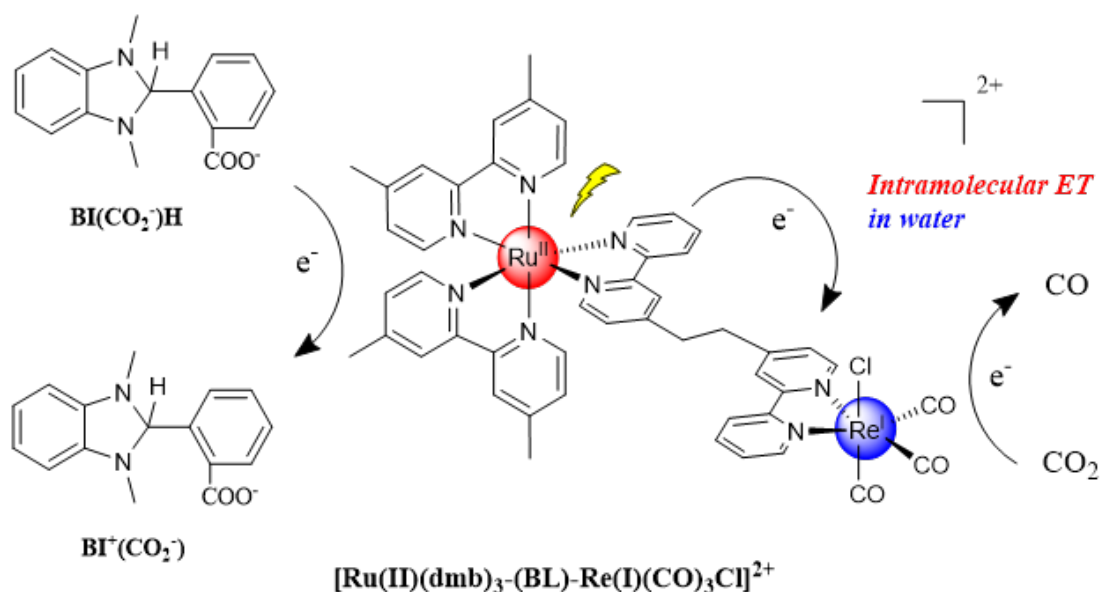
4

Figure 2: Mechanism of PIET process in Ru(II)-C_2H_2-Re(I) complex in the water phase for converting CO_2 to Co.

The potential energy curve computed for $[Ru^{II}(dmb)_2\text{-}(BL)\text{-}Re^I(CO)_3Cl]^{2+}$ complex (or $\mathbf{Ru^{II}-BL-Re^I}$) and PIET process of simple two-state adiabatic and non-adiabatic (diabatic) systems are shown in Figure 1. In both cases the $\mathbf{Ru^{II}-BL-Re^I}$ systems are represented in two states, that before electron transfer (the reactant state), and that after electron transfer (the product state). The difficulty of electron transferring depends on the Gibbs activation energy and nuclear displacement between two states.[10,11] Figure 2 shows a simple mechanism of single ET of $\mathbf{Ru^{II}-BL-Re^I}$ driven by light. $[Ru(dmb)_3]^{2+}$ specie was reduced by one electron from $BI(CO_2^-)H$ reductant.

2 Theory

2.1 Components of the Marcus equation

In this work, we address PIET by considering the Marcus theory in a picture of a diabatic state, where the constrained density functional theory (CDFT) that proposed by Wu and Van Voorhis.[10] CDFT is a generalization approach of DFT in which the external constraint is applied in order to simulate excitation processes and response properties. CDFT relies on the concept of adding additional constraint term of weight function with the strength of constraint potential $w(\mathbf{r})$ acting on specified region (Lagrange multiplier) V_c. The ground state energy of N-electrons system associated with solving constrained minimization/maximization problem is generally derived as follows

$$E\left[N\right] = \min_{\rho} \max_{\{V_c\}} \left[E^{\mathrm{KS}}[\rho(\mathbf{r})] + \sum_c V_c \left(\int w_c(\mathbf{r})\rho(\mathbf{r})\mathrm{d}\mathbf{r} - N_c \right) \right] \qquad (1)$$

where $\rho(\mathbf{r})$ is the electron density, E^{KS} is Kohn-Sham energy, c is the specified region, and N_c is the defined charge or spin multiplicity of the specified region.

While it has been shown that CDFT can be used to access the diabatic state, in which λ and H_{DA} have been computed directly, other chemical descriptions are additionally necessary to provide comprehensive insight in order to ensure that we have computed a desired diabatic state. Mulliken and Löwdin population analysis methods were used to compute the charge of redox species in order to confirm the existence of the charged-constrained state of $\mathbf{Ru^{II}-BL-Re^{I}}$. The dependence of BL distance on electronics communication between donor and acceptor was systematically investigated. Generally, the low λ is necessary for a fast forward ET process in the mixed-valence hybrid system.

The probability of ET between different sites, from donor to acceptor, during an

excited state, decreased with an increasing distance between these two sites. To quantify the energy that involves PIET, one must address the diabatic state of ET first. Then the existence of separation of reactant and product states can be found. Marcus equation has been enormously used to compute the rate of the kinetics of the PIET, given by Equation 2. The significant keys that dominate the kinetics involved in a unimolecular ET are identified by three terms of energy: the nuclear reorganization energy (λ), electron transfer matrix element, or electronics coupling energy (H_{DA}) between donor and acceptor, and the standard the Gibbs free energy (ΔG°). A generalized rate constant of electron transfer (k_{ET}) reads

$$k_{ET} = \frac{2\pi}{\bar{h}} H_{DA}^2 \frac{1}{\sqrt{4\pi\lambda k_B T}} exp\left[-\frac{(\lambda + \Delta G^\circ)^2}{4k_B T\lambda}\right] \tag{2}$$

with

$$H_{DA} = \frac{1}{(1 - S_{DA})}\left|V_{DA} - S_{DA}\frac{(H_{DD} + H_{AA})}{2}\right| \tag{3}$$

where λ is the energy required to change the structure of the complex resulting from the molecular rearrangement that occurs as the charge is distributed throughout the complex. H_{DA} indicates the ability of electronics communication when electron travel from donor to acceptor, which can be determined using Equation 3. The ΔG^* is determined by ΔG° and λ at thermodynamics temperature T. k_B is the Boltzmann constant.

We also compute H_{DA} using eigenstate-based and charge density-state-based methods including the generalized Mulliken-Hush (GMH),[12] maximum charge difference (FCD),[13] and direct coupling (DC) methods,[14–17] where abbreviated with GMH-H_{DA}, FCD-H_{DA}, and DC-H_{DA}, respectively. Both GMD-H_{DA} and FCD-H_{DA} are obtained from the time-dependent density functional theory (TD-DFT) calculation, whereas DC-H_{DA} method relies on ground-state DFT method. The GMH-H_{DA} can be computed as follows

$$H_{DA} = \frac{(E_j - E_i)\mu_{ij}}{\sqrt{(\mu_{ii} - \mu_{jj})^2 + 4\mu_{ij}^2}} \tag{4}$$

where E_i and E_j are energies for each pair of the ground state and excited state, and μ_{ii}, μ_{jj}, and μ_{ij} are transition dipole moments for different species (reactant state and product state). The in-house development of GMH module modified from the original version of the module in NWChem is available free of charge at `https://github.com/rangsimanketkaew/GMH` and distributed under the MIT license.

3 Computational details

All DFT and TD-DFT calculations were performed in Q-Chem 5.0[11] program package. For constructing adiabatic state of the system, ground state geometry optimizations were carried out using a long-range CAM-B3LYP functional in combination with 6-31G(d) and SDD-ECP, where the former was used to treat all atoms, whereas the latter was used for Ru and Re atoms.[18] All calculations included the approximation of the solvation effect of water ($\epsilon = 78.39$) using the COSMO model. For the diabatic state, where both symmetry and charge constraint was imposed during the calculation, we used the CDFT module in the development version of the NWChem 7.0.0 program package[19] for geometry optimization and to compute the inner nuclear reorganization energy (λ_{in}) and H_{DA} at the state of interest. In addition, we used GMH, FCD, and DC modules in Q-Chem, and our development version of ET module in combination with CDFT module in NWChem to compute H_{DA} of $\mathbf{Ru^{II}-BL-Re^{I}}$ complexes. Due to the PIET is largely dominated by the λ_{in}, therefore the λ_{out} is neglected. Population analysis methods including Mulliken and Löwdin were used to confirm the existence of the diabatic state of PIET.
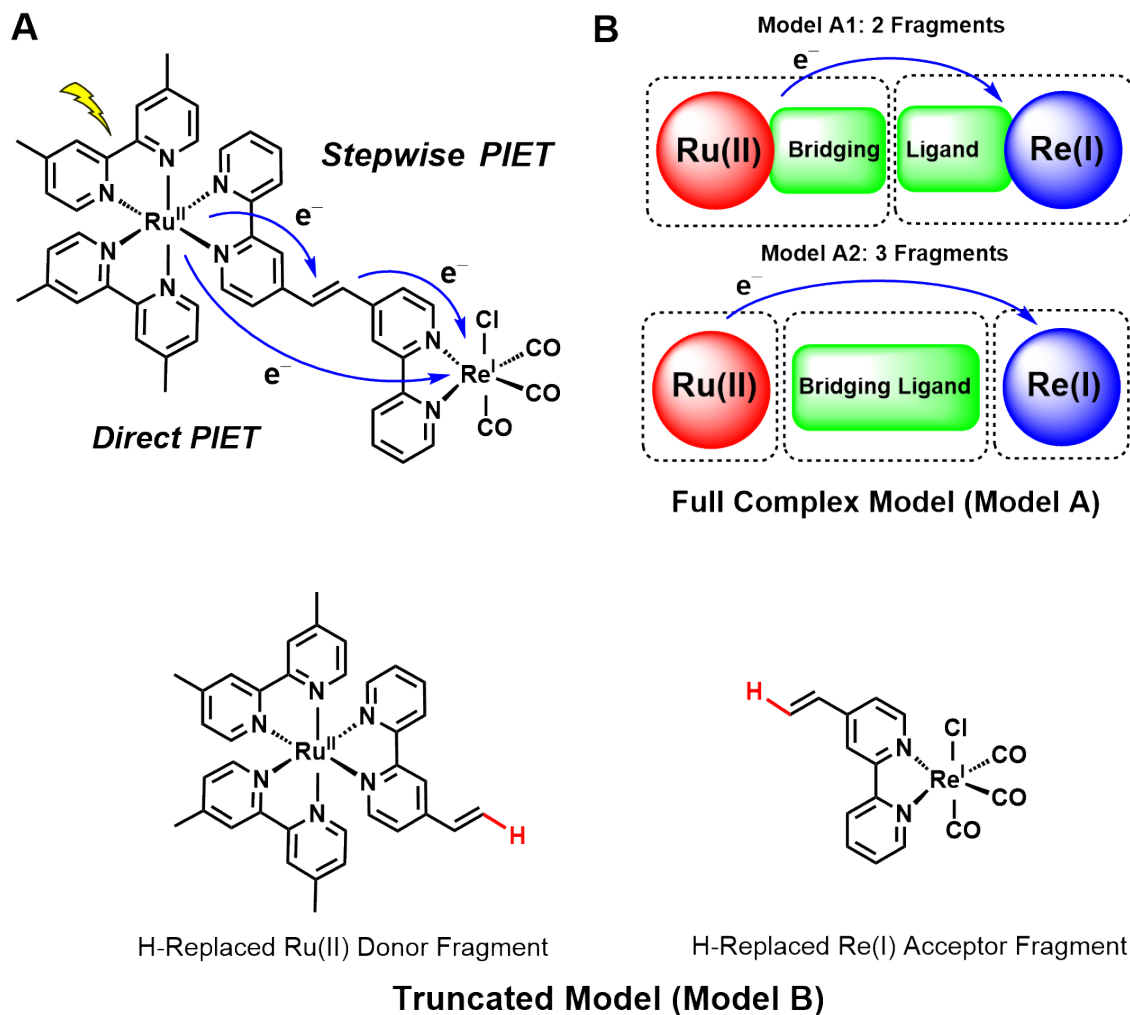
4 Molecular design

Figure 3: (A) Simple mechanism of stepwise and direct PIET processes. (B) 2-fragment (Model 2A) and 3-fragments (Model 2B) separation for full complex model.

The electronics state optimization of $\mathbf{Ru^{II}-BL-Re^{I}}$ complex has to correspond to the constrained state. In this work, we modeled the reactant and product states, which represent before and after electron transfer scenarios , by single electron transfer. Figure 3A shows the step-wise and direct mechanism of single electron transfer between Ru^{II} fragment and Re^{I} fragment through C_2H_2 as a bridging ligand. Figure 3B shows a simple scheme of 2-fragment (model 2A) and 3-fragment (model 2B) for the full complex model. The studied reaction is a

9

one-step ET process (from $Ru^{II}-BL^0-Re^I$ to $Ru^{III}-BL^0-Ru^0$) and the total net charge has not changed. The one-electron-doped $\mathbf{Ru^{II}-BL-Re^I}$ complex was considered for PIET. The transferring electron was localized on Ru in the reactant state and was localized on Re in the product state.

Single-electron transfer mechanism was proposed with so-called truncated and full complex models. We proposed two computational schemes for computing λ, comprised of a truncated model, where donor and acceptor are separate, and a full complex model, where charge localization is applied. For the truncated model (model 1), we replaced the whole Re^I fragment with a hydrogen atom to make up a donor fragment, and similarly, Ru^{II} fragment is replaced by a hydrogen atom to make up an acceptor. For the full complex model (model 2), the $\mathbf{Ru^{II}-BL-Re^I}$ complex was charge-separated divided into two (model 2A) and three (model 2B) fragments.
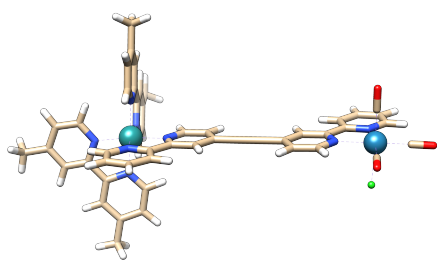
Table 1: Bridging ligand of each complex.

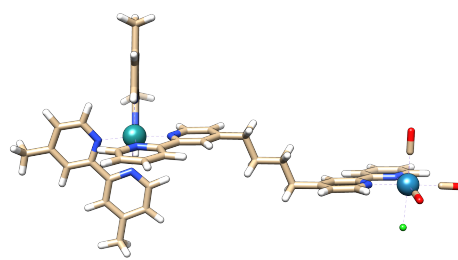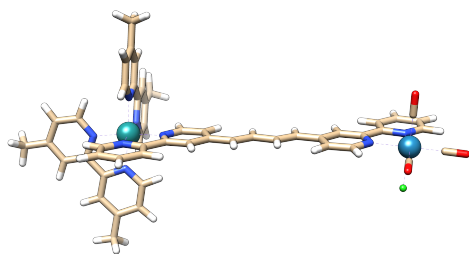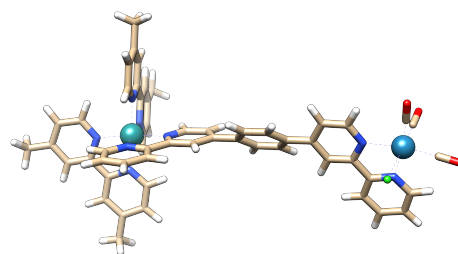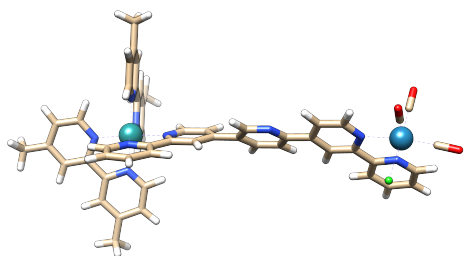| Complex	Bridging ligand
BL-1	$-CH_2-CH_2-$
BL-2	$-CH=CH-$
BL-3	$-C \equiv C-$
BL-4	$-CH_2-CH_2-CH_2-CH_2-$
BL-5	$-CH=CH-CH=CH-$
BL-6	$-Benzene-$
BL-7	$-Pyridine-$
BL-8	$-Biphenyl-$
BL-9	$-Bipyridine-$
BL-10	$-Napthalene-$
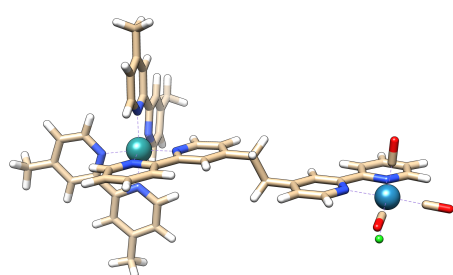
(a) BL-1
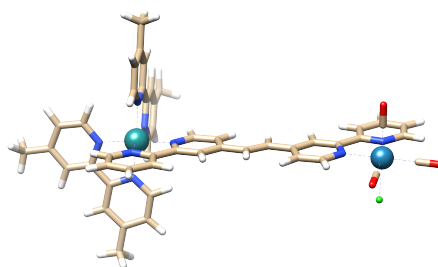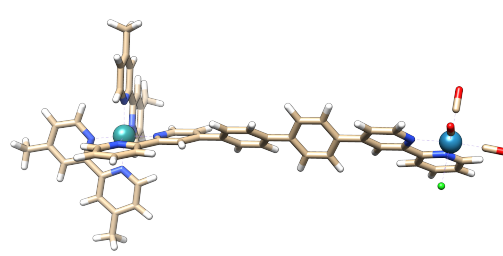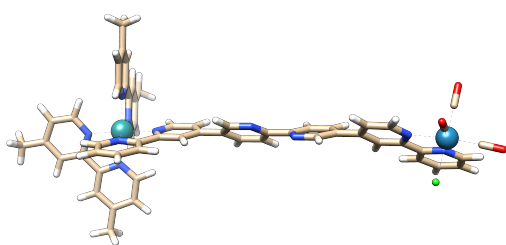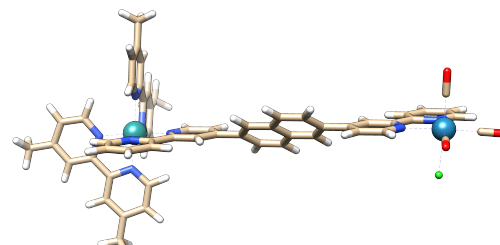
(b) BL-2

(c) BL-3

(d) BL-4

(e) BL-5

(f) BL-6

(g) BL-7

(h) BL-8

(i) BL-9

(j) BL-10

Figure 4: DFT-optimized structures of all Ru(II)-BL-Re(I) complexes. Frame order: from top to bottom and from left to right.

Figure 4 shows the optimized structures of all $\mathbf{Ru^{II}-BL-Re^{I}}$ complexes in the ground state.

5   Results and discussion

5.1   Nuclear reorganization energy calculation

We start this section with the calculation of reorganization energy λ, an important component in the Marcus equation. The λ is a minimum energy required to transform the system from one state to the other state.[20] Total reorganization energy (λ_{total}) is expressed as the sum of inner-sphere nuclear reorganization energy (λ_{in}) which accounts for a vibrational reorganization of the redox partners and outer-sphere reorganization energy (λ_{out}) which attributed to the reorganization of the solvent dipoles effect. Comparing the λ_{in} with the λ_{out}, the latter is generally small. Thus, we neglected λ_{out} for PIET.

We begin with the analytical generalization of standard inner reorganization energy[21] with the notation $E(a|b)$ which is used to represent the energy of the state a at the equilibrium structure b

$$\lambda_{in} = E(D^+A^-|DA) - E(D^+A^-|(D^+A^-) \tag{5}$$

where D and A are the donor and acceptor species where electron transferring starts and ends, respectively. For a truncated model, one can simply use Nelson's four-point method[22] to compute the λ_{in} of adiabatic system,

$$\lambda_{in} = E(D|D^+) - E(D^+|D^+) + E(A|A^-) - E(A^-|A^-) \tag{6}$$

12

It is obvious that the Equation 5 includes the connection between the donor and acceptor while Equation 6 lacks this connection. In order to investigate a comprehensive electronics description for PIET for a full complex model of Ru^{II} (donor) and Re^{I} (acceptor) fragments were linked by BL (see Figure 3), we in this work introduce the direct equation that combines all relevant donor and acceptor states to calculate accurate λ_{in},

$$\lambda_{in} = \lambda^{\pm}$$
$$= E_0 E_0(Q_+ Q_-) - E_0 E_0(Q_0 Q_0) + E_+ E_-(Q_0 Q_0) - E_+ E_-(Q_+ Q_-) \tag{7}$$

where $\lambda^{\pm}$ is hole/electron reorganization energy computed at charge localized/neutral geometry using CDFT method, E is single-point energy, and Q is an optimized geometry with the subscripts 0, +, and – denoting neutral, cationic, and anionic states, respectively.

Table 2: Computed inner nuclear reorganization energy (in meV) of $\mathbf{Ru^{II}-BL-Re^{I}}$ complex for full complex model 2A and model 2B.

Complex	Length of BL (Å)	Truncated model	Full complex model	
			Model 2A	Model 2B
BL-1	13.7	269	15.4	15.0
BL-2	16.1	225	14.4	14.9
BL-3	18.5	258	17.1	16.0
BL-4	20.9	273	18.2	18.0
BL-5	23.3	297	20.6	21.4

Table 2 reports the computed λ_{in} of $\mathbf{Ru^{II}-BL-Re^{I}}$ systems. The λ_{in} of the truncated model was much higher than both 2-fragment (model 2A) and 3-fragment (model 2B) full complex models. For the full complex model, model 2B yields the λ_{in} a little lower than the other. $\mathbf{Ru^{II}-BL_2-Re^{I}}$ complex gives the lowest λ_{in}, which means that this complex requires a little energy to change the geometry of complex from reactant state

to product state. Senevirathna et al. reported that a small λ_{in} is desirable for the high efficiency of photoinduced electron transfer.[23]

The λ_{in} was computed by using model 1, model 2A, and model 2B. The λ_{in} of model 1 was at least 1 order of magnitude higher than model 2A and model 2B. Model 2B yielded the λ_{in} lower than the other. $\mathbf{Ru^{II}-BL_2-Re^{I}}$ complex provided the lowest λ_{in} among others. This result indicates that the BL-2 complex, compared to others, requires the lowest energy to change the geometry from reactant state to product state during PIET. These computational results show that good predictions of the λ_{in} in $\mathbf{Ru^{II}-BL-Re^{I}}$ complexes were achieved by using the full complex model, especially model 2B (3-fragment model).

5.2 Electron transfer matrix element calculation

The low λ in is not only needed for fast forward electron transfer, but we also considered electron transfer matrix element (H_{DA}) that implies electronic communication between two sides of a hybrid system.[24] We were not able to compute H_{DA} for a truncated model because the calculation of charged localization was not be accomplished with a conventional DFT. Therefore, the other choice for considering the charge localization is a full complex model. We considered model 2A and model 2B and found that BL-2 system yields the highest H_{DA} instead of BL-1 system. We attributed this unexpected result to electron delocalization in a π-conjugated bridge to the kinetics of PIET. The reason is, for a too short bridge, the electron can possibly transfer from Re^{I} fragment back to Ru^{II} fragment. This led the diabatic state of PIET to undergo the inverted Marcus region of PIET, which decreases H_{DA}.[24] The computed H_{DA} of $\mathbf{Ru^{II}-BL-Re^{I}}$ complexes were found to be around $300-700$ in meV. A model 2A has H_{DA} higher than that computed by model 2B. The computational results also show that electrons can directly travel from Ru^{II} fragment to Re^{I} fragment. The $\mathbf{Ru^{II}-BL_2-Re^{I}}$ complex yields the highest computed H_{DA} compared to other complexes. From ET theory,

the rate of PIET is increased when the low reorganization energy and the high H_{DA} were together received.

The computed H_{DA} of BL-5 is lower than that of BL-1. The accessibility of BL is an available lone pair electron that controls the rate of ET. Moreover, to our knowledge, the computational results show that the self-interaction error in conventional DFT may cause incorrect estimation of H_{DA} of neutral, reduced, and oxidized molecules for the ground state.[25,26] A more quantitative prediction was provided by CDFT calculations, which is reported in Table 3. Electron delocalization simply occurs in an unsaturated C=C bridging ligand, however, we found that the electronic communication is weak for the longer bridging ligand structure, suggesting that the conventional DFT predictions have the wrong behavior.

Table 3: Computed electron transfer matrix element (in meV) of $\mathbf{Ru^{II}-BL-Re^{I}}$ complexes using CDFT calculation.

Complex	Length of BL (Å)	Full complex model	
		2-fragments (Model 2A)	3-fragment (Model 2B)
BL-1	13.7	643	426
BL-2	16.1	749	436
BL-3	18.5	555	353
BL-4	20.9	500	344
BL-5	23.3	438	307

Table 4: Computed electron transfer matrix elements (in meV) of $\mathbf{Ru^{II}-BL-Re^{I}}$ complex for different electron transfer models using maximum charge differences (FCD), generalized Mulliken-Hush (GMH), and 1+1, Relaxed, and FMO direct coupling (DC) methods. Note that calculation that failed after several attempts stated with -.

Complex	FCD	GMH	DC		
			1+1	Relaxed	FMO
BL-1	923	834	264	1076	360
BL-2	902	810	233	954	351
BL-3	872	798	205	874	327
BL-4	825	768	181	840	-
BL-5	-	751	175	-	-

Wavefunction-based methods including FCD, GMH, and DC methods were used to compute H_{DA}, as reported in Table 4. The computed H_{DA} decreased when BL is longer. Moreover, when the H_{DA} is sufficiently small ($H_{DA} \leq 500$ meV), the precursor hybrid complex can favorably take some thermal energy from the surrounding and jump from one potential energy curve to the other.[24,26] The rate of the diabatic PIET, in this case, was considerably reduced and is not governed by the inner nuclear reorganization.
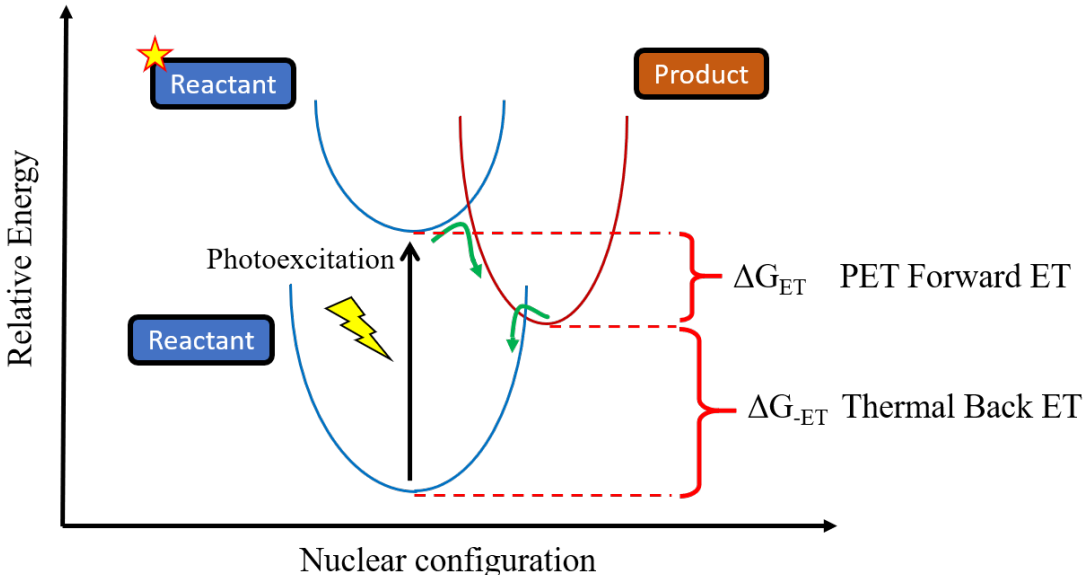

Figure 5: Potential energy landscape of photoinduced electron transfer. Normal and inverted Marcus regions are highlighted in red and green. D and D* denote the donor in the ground and excited states, respectively, and A is the acceptor in the ground state. ΔG is the Gibbs energy between local minima of each state.

Table 5: Computed rate constant of PIET (in s^{-1}) of Ru$-$CH$_2$CH$_2$$-$Re (BL5) hybrid complex. k$_{Et}$ cinluding λ_{out} is in parenthesis.

Complex	Model 1 (DFT)		Model 2A (CDFT)		Model 2B (CDFT)	
	Gas	Water	Gas	Water	Gas	Water
Ru$-$CH$_2$CH$_2$$-$Re	8.4 x 10^7	2.6 x 10^6 (2.5 x 10^6)	3.5 x 10^5	4.4 x 10^4 (1.2 x 10^6)	1.5 x 10^5	1.4 x 10^5 (2.5 x 10^6)

In practical applications of a mixed-valence compound for fast forward photoinduced intramolecular electron transfer process depends on the direction of the electron

transfer process. Figure 5 shows the ET process in diabatic for the normal and inverted Marcus regions, where refers to forward and backward ET in the excited state. Charge separation of $\mathbf{Ru^{II}-BL-Re^{I}}$ complex in normal Marcus region has to be maintained during a period of time sufficient for further single ET reaction to take place. With high H_{DA} and low Gibbs activation energy, it is likely that fast forward ET involving an excited state has to be as a fast as possible, while backward ET during charges recombination has to be slow. Otherwise, electron transfer will occur in an inverted Marcus region.

5.3 Molecular bonding analysis

Table 6: Mulliken and Löwdin charge analysis on the diabatic state for truncated model and full complex model, and for DFT and CDFT calculations.

Method	Complex	Truncated model (DFT)		Full complex 2A (CDFT)		Full complex 2B (CDFT)		
		Ru(II)	Re(I)	Ru(II)	Re(I)	Ru(II)	Bridge	Re(I)
Mulliken	BL-1	1.958	0.042	2.032	-0.032	2.018	0.009	-0.027
	BL-2	1.153	0.847	2.157	-0.157	2.142	-0.044	-0.098
	BL-3	1.644	0.356	2.149	-0.149	2.137	-0.052	-0.085
	BL-4	1.502	0.498	2.008	-0.008	1.987	0.056	-0.043
	BL-5	1.356	0.644	2.122	-0.112	2.043	0.086	-0.129
Löwdin	BL-1	1.106	0.894	2.106	-0.106	2.024	-0.006	-0.018
	BL-2	1.207	0.793	2.032	-0.032	2.035	0.021	-0.056
	BL-3	1.306	0.694	2.095	-0.095	1.98	0.042	-0.022
	BL-4	1.225	0.775	2.115	-0.115	2.083	0.002	-0.085
	BL-5	1.156	0.844	2.214	-0.214	2.104	-0.016	-1.998

To analyze the charged localization on $\mathbf{Ru^{II}-BL-Re^{I}}$ complexes for before and after electron transfer, the population analysis was considered. Table 6 reports the computed charge localization in $\mathbf{Ru^{II}-BL-Re^{I}}$ complex for the diabatic state by using Mulliken and Löwdin methods. The total net charge of Ru^{II}, BL, and Re^{I} fragments was presumed to be 2, 0, and 0, respectively. When it comes to the comparison of DFT and CDFT calculations, we found that CDFT predicted the diabatic state accurately rather than DFT. Model 2A and model 2B show the accurate charge localized states for Ru^{II}, BL, and Re^{I} fragments.

(a) BL-1

(b) BL-1

(c) BL-2

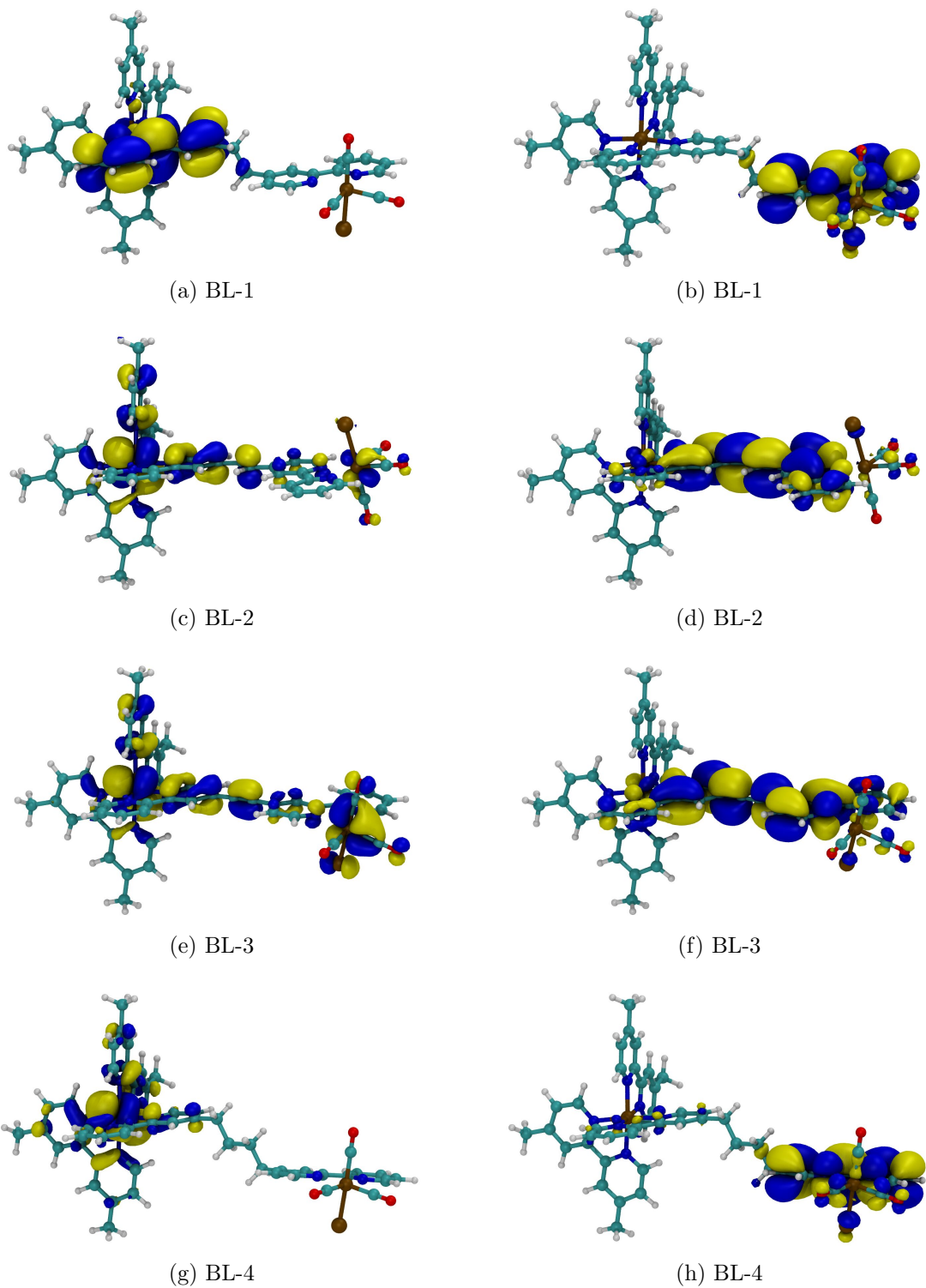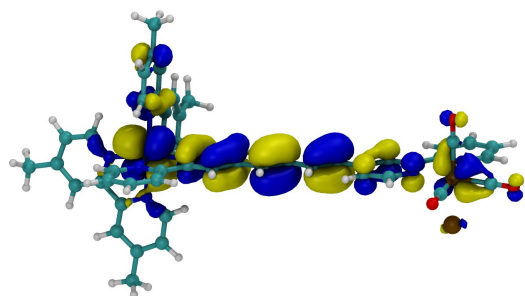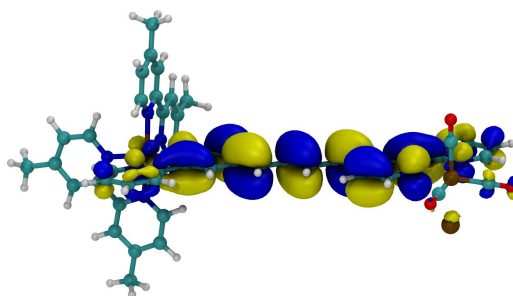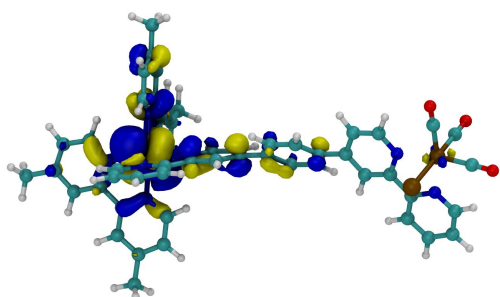(d) BL-2

(e) BL-3

(f) BL-3

(g) BL-4

(h) BL-4

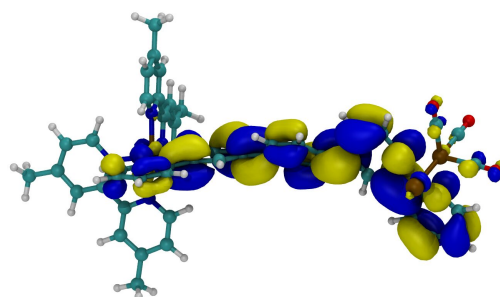Figure 6: Frontier molecular orbitals (HOMO (left) and LUMO (right)) of all Ru(II)-BL-Re(I) complexes computed at TD-DFT/CAM-B3LYP/6-31G(d)/SDD in water phase.
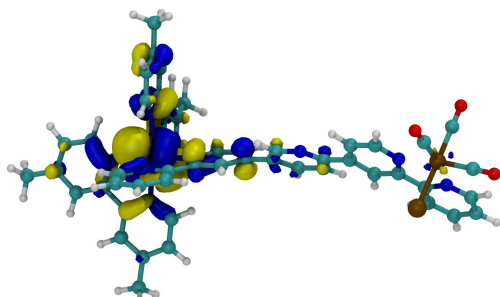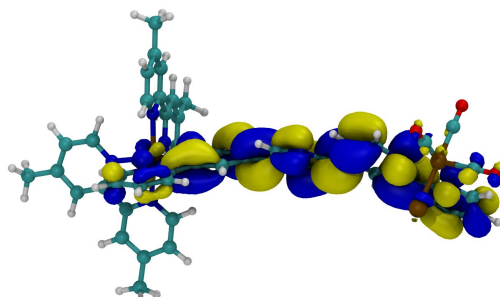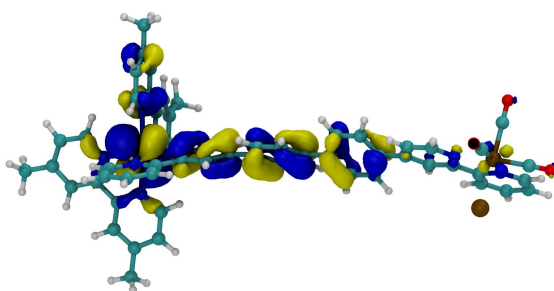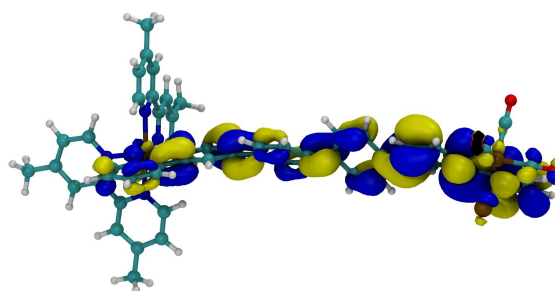
(i) BL-5

(j) BL-5

(k) BL-6

(l) BL-6

(m) BL-7

(n) BL-7

(o) BL-8

(p) BL-8

Figure 5: Frontier molecular orbitals (HOMO (left) and LUMO (right)) of all Ru(II)-BL-Re(I) complexes computed at TD-DFT/CAM-B3LYP/6-31G(d)/SDD in water phase.

(q) BL-9

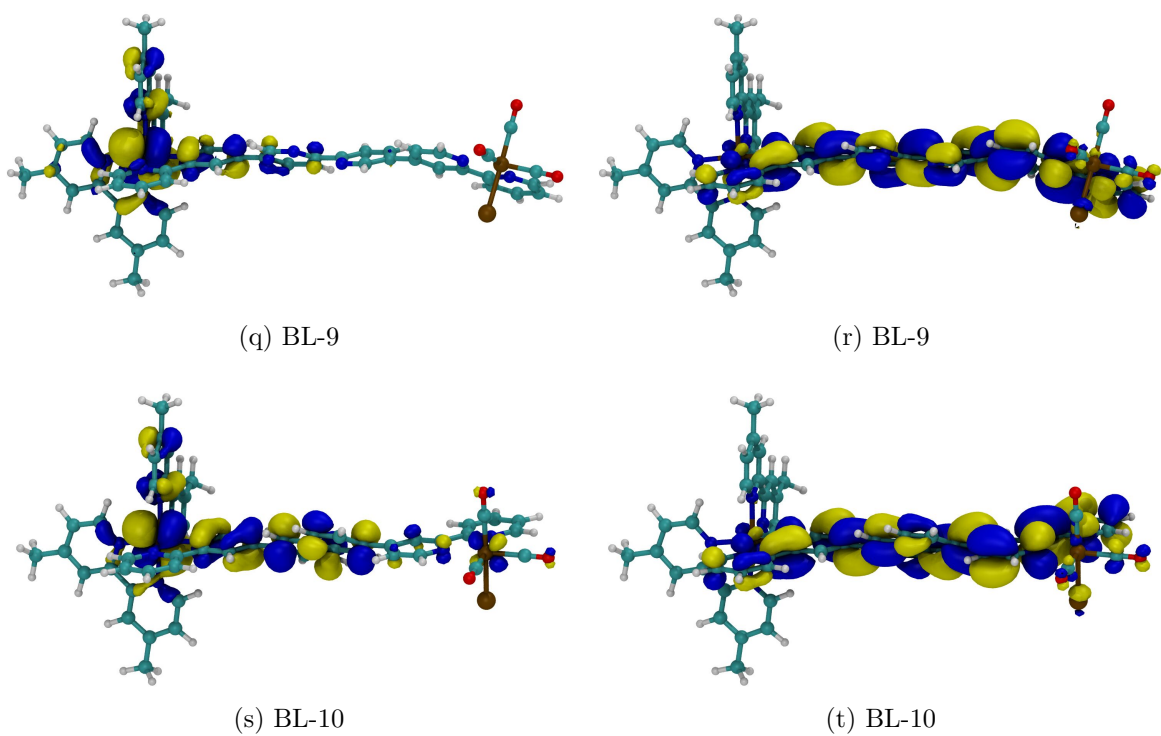(r) BL-9

(s) BL-10

(t) BL-10

Figure 5: Frontier molecular orbitals (HOMO (left) and LUMO (right)) of all Ru(II)-BL-Re(I) complexes computed at TD-DFT/CAM-B3LYP/6-31G(d)/SDD in water phase.
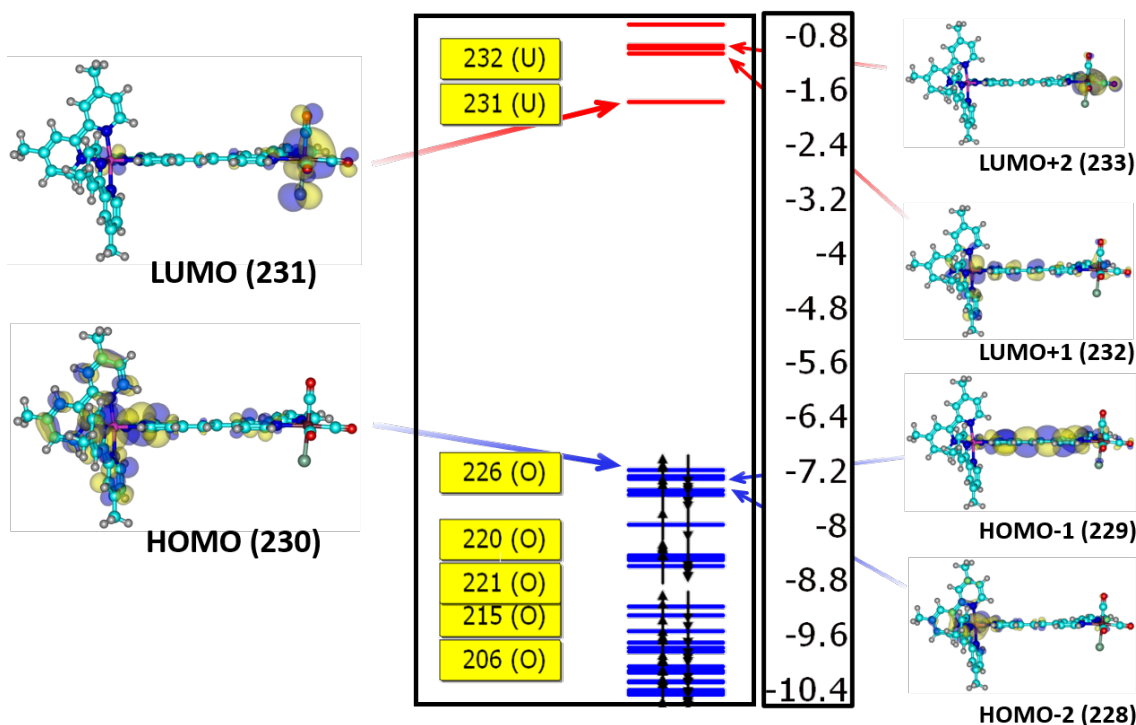
Figure 6: Selected MOs energy levels. Energies are in eV.

Frontier molecular orbitals were computed to display the electron density for reactant and product states, as shown in Figure 6. The highest occupied molecular orbital (HOMO) reveals that the electron density of the system is mostly dominated by Ru^{II} fragment in the ground state. When the $\mathbf{Ru^{II}-BL-Re^{I}}$ complex was excited, single-electron transferred from Ru^{II} fragment to Re^{I} fragment through BL. Singly occupied molecular orbitals (SOMOs) were calculated to describe the role of π-conjugated diene in PIET. The computational results clearly show that MOs confirm forward electron transfer for the diabatic state. Moreover, the energy gap between HOMO and SOMO of all complexes is almost the same, corresponding to internal electronic communication. Therefore, the $\mathbf{Ru^{II}-BL-Re^{I}}$ complex can be promoted to high efficient BL such as BL-1 and BL-2 system was found that it can be a promising efficient electron transfer mixed-valence complex.

6 Conclusion

We study photoinduced intramolecular electron transfer (PIET) of hybrid mixed-valence complexes using computational method. We propose a computational workflow for studying the electron transfer in $\mathbf{Ru^{II}-Re^{I}}$ complexes. Constrained density functional theory is used to investigate the rate of PIET process in $\mathbf{Ru^{II}-BL-Re^{I}}$ hybrid complexes, where BL is a family of organic molecule containing conjugated diene systems. We compute the inner nuclear reorganization energy (λ_{in}), electron transfer matrix element between donor and acceptor (H_{DA}), and population analysis of covalent $\mathbf{Ru^{II}-BL-Re^{I}}$ complex. At this stage, the non-adiabatic (or diabatic) state of the studied system was studied using charged localization approach. Our proposed model for simple PIET including truncated model (model 1) and full complex model, including 2-fragment model as model 2A, and 3-fragment model as model 2B, have been used for $\mathbf{Ru^{II}-BL-Re^{I}}$ complexes. A good agreement between the two models was obtained over a range of complex geometries. Either method could be applied at an arbitrary nuclear geometry and, as computational results, may be used to calculate λ and H_{DA} of PIET. The series of π-conjugated diene bridging ligand, corresponding H_{DA} as a function of the distance between donor and acceptor, were observed for reactant and product state. A full complex model yields a natural definition of electron transfer distance, in contrast to a truncated model, which represented an independent against the PIET. The Model 2B yields H_{DA} less than model 2A. In addition to calculations of the Marcus equation's components, we carefully examined the frontier molecular orbitals, including HOMO, LUMO, and SOMO, for reaction and product state of the system to verify the existence of electron localization in the diabatic state and to determine which orbitals are involved in the electron transfer. Our computational results also reveal that the low inner nuclear reorganization energy is required for further development of an efficient electron transfer hybrid complex.

Acknowledgement

References

(1) Perutz, R. N.; Procacci, B. Photochemistry of Transition Metal Hydrides. *Chemical Reviews* **2016**, *116*, 8506–8544.

(2) Parasram, M.; Gevorgyan, V. Visible light-induced transition metal-catalyzed transformations: beyond conventional photosensitizers. *Chemical Society Reviews* **2017**, *46*, 6227–6240.

(3) Begum, A.; Pickup, P. G. Electrocatalysis of CO2 reduction by ruthenium benzothiazole and bithiazole complexes. *Electrochemistry Communications* **2007**, *9*, 2525–2528.

(4) Kuramochi, S.; Newton, G. N.; Shiga, T.; Oshio, H. Electrochemical Carbon Dioxide Reduction Catalyzed by a Dinuclear Ruthenium Complex with a Flexible Bridging Ligand. *Chemistry Letters* **2014**, *43*, 1222–1223.

(5) Prier, C. K.; Rankic, D. A.; MacMillan, D. W. C. Visible Light Photoredox Catalysis with Transition Metal Complexes: Applications in Organic Synthesis. *Chemical Reviews* **2013**, *113*, 5322–5363.

(6) Suntharalingam, K.; White, A. J. P.; Vilar, R. Two Metals Are Better than One: Investigations on the Interactions between Dinuclear Metal Complexes and Quadruplex DNA. *Inorganic Chemistry* **2010**, *49*, 8371–8380.

(7) Gholamkhass, B.; Mametsuka, H.; Koike, K.; Tanabe, T.; Furue, M.; Ishitani, O. Architecture of Supramolecular Metal Complexes for Photocatalytic CO2 Reduction: RutheniumRhenium Bi- and Tetranuclear Complexes. *Inorganic Chemistry* **2005**, *44*, 2326–2336.

(8) Sato, S.; Koike, K.; Inoue, H.; Ishitani, O. Highly efficient supramolecular photocatalysts for CO $_2$ reduction using visible light. *Photochem. Photobiol. Sci.* **2007**, *6*, 454–461.

(9) Nakada, A.; Koike, K.; Maeda, K.; Ishitani, O. Highly efficient visible-light-driven CO2 reduction to CO using a Ru(II)–Re(I) supramolecular photocatalyst in an aqueous solution. *Green Chemistry* **2016**, *18*, 139–143.

(10) Wu, Q.; Van Voorhis, T. Direct optimization method to study constrained systems within density-functional theory. *Physical Review A* **2005**, *72*.

(11) Shao, Y.; Gan, Z.; Epifanovsky, E.; Gilbert, A. T. B.; Wormit, M.; Kussmann, J.; Lange, A. W.; Behn, A.; Deng, J.; Feng, X.; Ghosh, D.; Goldey, M.; Horn, P. R.; Jacobson, L. D.; Kaliman, I.; Khaliullin, R. Z.; Kuś, T.; Landau, A.; Liu, J.; Proynov, E. I.; Rhee, Y. M.; Richard, R. M.; Rohrdanz, M. A.; Steele, R. P.; Sundstrom, E. J.; III, H. L. W.; Zimmerman, P. M.; Zuev, D.; Albrecht, B.; Alguire, E.; Austin, B.; Beran, G. J. O.; Bernard, Y. A.; Berquist, E.; Brandhorst, K.; Bravaya, K. B.; Brown, S. T.; Casanova, D.; Chang, C.-M.; Chen, Y.; Chien, S. H.; Closser, K. D.; Crittenden, D. L.; Diedenhofen, M.; Jr, R. A. D.; Do, H.; Dutoi, A. D.; Edgar, R. G.; Fatehi, S.; Fusti-Molnar, L.; Ghysels, A.; Golubeva-Zadorozhnaya, A.; Gomes, J.; Hanson-Heine, M. W. D.; Harbach, P. H. P.; Hauser, A. W.; Hohenstein, E. G.; Holden, Z. C.; Jagau, T.-C.; Ji, H.; Kaduk, B.; Khistyaev, K.; Kim, J.; Kim, J.; King, R. A.; Klun-

zinger, P.; Kosenkov, D.; Kowalczyk, T.; Krauter, C. M.; Lao, K. U.; Laurent, A. D.; Lawler, K. V.; Levchenko, S. V.; Lin, C. Y.; Liu, F.; Livshits, E.; Lochan, R. C.; Luenser, A.; Manohar, P.; Manzer, S. F.; Mao, S.-P.; Mardirossian, N.; Marenich, A. V.; Maurer, S. A.; Mayhall, N. J.; Neuscamman, E.; Oana, C. M.; Olivares-Amaya, R.; O'Neill, D. P.; Parkhill, J. A.; Perrine, T. M.; Peverati, R.; Prociuk, A.; Rehn, D. R.; Rosta, E.; Russ, N. J.; Sharada, S. M.; Sharma, S.; Small, D. W.; Sodt, A.; Stein, T.; Stück, D.; Su, Y.-C.; Thom, A. J. W.; Tsuchimochi, T.; Vanovschi, V.; Vogt, L.; Vydrov, O.; Wang, T.; Watson, M. A.; Wenzel, J.; White, A.; Williams, C. F.; Yang, J.; Yeganeh, S.; Yost, S. R.; You, Z.-Q.; Zhang, I. Y.; Zhang, X.; Zhao, Y.; Brooks, B. R.; Chan, G. K. L.; Chipman, D. M.; Cramer, C. J.; III, W. A. G.; Gordon, M. S.; Hehre, W. J.; Klamt, A.; III, H. F. S.; Schmidt, M. W.; Sherrill, C. D.; Truhlar, D. G.; Warshel, A.; Xu, X.; Aspuru-Guzik, A.; Baer, R.; Bell, A. T.; Besley, N. A.; Chai, J.-D.; Dreuw, A.; Dunietz, B. D.; Furlani, T. R.; Gwaltney, S. R.; Hsu, C.-P.; Jung, Y.; Kong, J.; Lambrecht, D. S.; Liang, W.; Ochsenfeld, C.; Rassolov, V. A.; Slipchenko, L. V.; Subotnik, J. E.; Voorhis, T. V.; Herbert, J. M.; Krylov, A. I.; Gill, P. M. W.; Head-Gordon, M. Advances in molecular quantum chemistry contained in the Q-Chem 4 program package. *Molecular Physics* **2015**, *113*, 184–215.

(12) Cave, R. J.; Newton, M. D. Generalization of the Mulliken-Hush treatment for the calculation of electron transfer matrix elements. *Chemical Physics Letters* **1996**, *249*, 15–19.

(13) Voityuk, A. A.; Rösch, N. Fragment charge difference method for estimating donor–acceptor electronic coupling: Application to DNA -stacks. *The Journal of Chemical Physics* **2002**, *117*, 5607–5616.

(14) Ohta, K.; Closs, G. L.; Morokuma, K.; Green, N. J. Stereoelectronic effects in intramolecular long-distance electron transfer in radical anions as predicted by ab-initio MO calculations. *Journal of the American Chemical Society* **1986**, *108*, 1319–1320.

(15) Broo, A. Electronic structure of donor-spacer-acceptor molecules of potential interest for molecular electronics. I. Donor--spacer-acceptor. *Chemical Physics* **1993**, *169*, 135–150.

(16) Zhang, L. Y.; Friesner, R. A.; Murphy, R. B. Ab initio quantum chemical calculation of electron transfer matrix elements for large molecules. *The Journal of Chemical Physics* **1997**, *107*, 450–459.

(17) Farazdel, A.; Dupuis, M.; Clementi, E.; Aviram, A. Electric-field induced intramolecular electron transfer in spiro .pi.-electron systems and their suitability as molecular electronic devices. A theoretical study. *Journal of the American Chemical Society* **1990**, *112*, 4206–4214.

(18) Yanai, T.; Tew, D. P.; Handy, N. C. A new hybrid exchange–correlation functional using the Coulomb-attenuating method (CAM-B3LYP). *Chemical Physics Letters* **2004**, *393*, 51–57.

(19) Valiev, M.; Bylaska, E. J.; Govind, N.; Kowalski, K.; Straatsma, T. P.; Van Dam, H. J. J.; Wang, D.; Nieplocha, J.; Apra, E.; Windus, T. L.; de Jong, W. A. NWChem: A comprehensive and scalable open-source solution for large scale molecular simulations. *Computer Physics Communications* **2010**, *181*, 1477–1489.

(20) Wander, M. C. F.; Kerisit, S.; Rosso, K. M.; Schoonen, M. A. A. Kinetics of Triscarbonato Uranyl Reduction by Aqueous Ferrous Iron: A Theoretical Study. *The Journal of Physical Chemistry A* **2006**, *110*, 9691–9701.

(21) Wu, Q.; Voorhis, T. V. Direct Calculation of Electron Transfer Parameters through Constrained Density Functional Theory. *The Journal of Physical Chemistry A* **2006**, *110*, 9212–9218.

(22) Nelsen, S. F.; Blackstock, S. C.; Kim, Y. Estimation of inner shell Marcus terms for

amino nitrogen compounds by molecular orbital calculations. *Journal of the American Chemical Society* **1987**, *109*, 677–682.

(23) Senevirathna, W.; Daddario, C. M.; Sauvé, G. Density Functional Theory Study Predicts Low Reorganization Energies for Azadipyrromethene-Based Metal Complexes. *The Journal of Physical Chemistry Letters* **2014**, *5*, 935–941.

(24) Ding, F.; Wang, H.; Wu, Q.; Van Voorhis, T.; Chen, S.; Konopelski, J. P. Computational Study of Bridge-Assisted Intervalence Electron Transfer. *The Journal of Physical Chemistry A* **2010**, *114*, 6039–6046.

(25) Bao, J. L.; Gagliardi, L.; Truhlar, D. G. Self-Interaction Error in Density Functional Theory: An Appraisal. *The Journal of Physical Chemistry Letters* **2018**, *9*, 2353–2358.

(26) Dreuw, A.; Head-Gordon, M. Failure of Time-Dependent Density Functional Theory for Long-Range Charge-Transfer Excited States: The Zincbacteriochlorin-Bacteriochlorin and Bacteriochlorophyll-Spheroidene Complexes. *Journal of the American Chemical Society* **2004**, *126*, 4007–4016.